1-1-2012

A simple noniterative principal component technique for rapid noise reduction in parallel MR images

Anand S. Patel
University of California, San Francisco

Qi Duan
NYU Langone Health

Philip M. Robson
Harvard Medical School

Charles A. McKenzie
Western University, cmcken@uwo.ca

Daniel K. Sodickson
NYU Langone Health

Published in final edited form as:
NMR Biomed. 2012 January ; 25(1): 84–92. doi:10.1002/nbm.1716.

A simple noniterative principal component technique for rapid noise reduction in parallel MR images

Anand S. Patel[a,*], **Qi Duan**[b], **Philip M. Robson**[c], **Charles A. McKenzie**[d], and **Daniel K. Sodickson**[b]

[a]Department of Radiology and Biomedical Imaging, University of California, San Francisco, CA, USA

[b]Center for Biomedical Imaging, Department of Radiology, New York University Medical Center, New York, NY, USA

[c]Department of Radiology, Beth Israel Deaconess Medical Center and Harvard Medical School, Boston, MA, USA

[d]Department of Medical Biophysics, University of Western Ontario, London, ON, Canada

Abstract

The utilization of parallel imaging permits increased MR acquisition speed and efficiency; however, parallel MRI usually leads to a deterioration in the signal-to-noise ratio when compared with otherwise equivalent unaccelerated acquisitions. At high accelerations, the parallel image reconstruction matrix tends to become dominated by one principal component. This has been utilized to enable substantial reductions in *g*-factor-related noise. A previously published technique achieved noise reductions via a computationally intensive search for multiples of the dominant singular vector which, when subtracted from the image, minimized joint entropy between the accelerated image and a reference image. We describe a simple algorithm that can accomplish similar results without a time-consuming search. Significant reductions in *g*-factor-related noise were achieved using this new algorithm with *in vivo* acquisitions at 1.5 T with an eight-element array.

Keywords

parallel MRI; signal processing; noise reduction; *g*-factor; SENSE; joint entropy; principal component analysis; artifact correction

INTRODUCTION

The scan time reductions afforded by parallel imaging are well known to come at the cost of noise amplifications characterized by the *g*-factor (1). Noise amplification can corrupt image quality and effectively limit maximal practical acceleration. Methods such as noise normalization and regularization techniques for reducing *g*-factor-related noise have been proposed in the past, but with mixed results. Noise normalization decreases noise by adaptively adjusting the amount of filtering for MR images acquired with inhomogeneous coils at the cost of nonuniform noise amplifications (2). Automatic Tikhonov regularization

[*]Correspondence to: A. S. Patel, Department of Radiology and Biomedical Imaging, University of California, San Francisco, 505 Parnassus Avenue, San Francisco, CA 94143-0628, USA. anand.patel@ucsf.edu.

balances tolerance to noise against additive bias to the result, improving image quality at the expense of potential changes to underlying image content (3).

Recently, a promising method was proposed for the reduction of *g*-factor-related noise (4), taking advantage of the fact that, for acceleration factors approaching the number of coils, the parallel image reconstruction matrix tends to be dominated by one singular value and vector. Larkman *et al*. (4) suggested that a search should be made for a multiple of the dominant singular vector which, when subtracted from the image, minimized the joint entropy (JE) between the accelerated image and a reference image. This algorithm is attractive because its ability to reduce noise improves as the acceleration factor increases, while preventing simple replication of the reference image; however, the JE method is computationally intensive, with reconstructions that can occupy several hours. We propose a method that uses a similar principal component approach, but eliminates the need for an exhaustive search, yielding results similar to the JE approach in a single straightforward step. This simple algorithm, which may be executed in real time as images are acquired and reconstructed, should allow significant reductions in *g*-factor-related noise for highly accelerated scans with the aid of a reference image of similar contrast.

THEORY

Principal component-based noise reduction

Appendix A provides a derivation of the sensitivity encoding (SENSE) method and the factorization of the encoding matrix (Equations [11]–[15]). The technique proposed by Larkman *et al*. (4,5) used an exhaustive search to find the value of the single dominant δS_k, defined in Appendix A, which minimized JE between the resultant image and a reference image. We propose that, by algebraically solving for δS_k, using least-squares fitting to a reference image, we can obtain similar results to the JE search, but in a fast and computationally efficient manner (6). In particular, for one dominant singular value, we can write:

$$\mathrm{x}'_{\text{Noise Reduced}} = \mathrm{x} - (s_1 \delta S_1)\, \mathrm{v}_1 \qquad [1]$$

By substituting a known low-resolution reference image $\mathbf{x_{ref}}$ to approximate the unknown $\mathrm{x}'_{\text{Noise Reduced}}$, we can arrive at the Moore-Penrose least-squares solution:

$$\delta S_{\text{ref}} \approx s_1 \left(\mathrm{v}_1 \cdot (\mathrm{x} - \mathrm{x}_{\text{ref}})\right) \qquad [2]$$

Thus, we can calculate the final expression for our least-squares noise-reduced (LSNR) image as:

$$\mathrm{x}'_{\text{LSNR}} = \mathrm{x} - \left(s_1^{-1} \delta S_{\text{ref}}\right) \mathrm{v}_1 \qquad [3]$$

Generalization to multiple values of δS_k is trivial, with $\mathbf{v}_1$ being replaced by a weighted sum over a larger subset of the columns of *V*.

For either the exhaustive search or the algebraic solution for the value of δS_k, there is a legitimate concern that the noise reduction method will simply replicate prior knowledge of the object as reflected in the reference image. This occurrence is protected against by the coupling of pixel intensities at aliasing positions; however, artifacts from the reference image may still enter the target image based on the derivations below. The pixel intensities

in the reference image-dependent vector $\left(s_1^{-1}\delta S_{\text{Ref}}\right)v_1$ subtracted from the reconstructed image are weighted by a single value, so that pixel intensities may not be manipulated independently and pixel-by-pixel replication of the reference image will not occur. Indeed, the precise degree to which reference image information can enter into the LSNR reconstruction may be obtained by substituting Equation [2] into Equation [3] and, from Equations [11] and [14], we arrive at the following form:

$$x'_{\text{LSNR}} = \Sigma_{k\neq 1} s_k^{-1} (v_k \otimes (u_k \cdot s)) + s_1^{-1} (v_k \otimes (u_1 \cdot s_{\text{ref}})) \quad [4]$$

Here, we can see that the projection $\mathbf{u}_1 \cdot \mathbf{s}_{\text{ref}}$ of the aliased reference signal $\mathbf{s}_{\mathbf{ref}}$ against the singular vector $\mathbf{u}_1$ directly replaces the true, but noisy, signal projection $\mathbf{u}_1 \cdot \mathbf{s}$ as a multiple of the singular vector $\mathbf{v}_1$. We note that $\mathbf{s}_{\mathbf{ref}}$ is characterized in a manner similar to $\mathbf{s}$ as seen in Equation [13]. Subtracting the true image x' from the LSNR-reconstructed image x'_{LSNR} in Equation [4] yields a difference:

$$x'_{\text{LSNR}} - x' = \left\{s_1^{-1} (v_1 \otimes u_1 \cdot (s'_{\text{ref}} - s'))\right\} + \left\{s_1^{-1} (v_1 \otimes (u_1 \cdot dS_{\mathbf{ref}})) + \Sigma_{k\neq 1} s_k^{-1} (v_k \otimes (u_k \cdot dS))\right\}$$

[5]

The first term in curly brackets in Equation [5] represents an artifact term, resulting from the projection of the difference between the reference and the true aliased signals against $\mathbf{u}_1$. The second term in curly brackets represents the residual noise, which is made up of any noise in the reference signal projected against $\mathbf{u}_1$ plus the remaining noise terms for uncorrected principal components. If the reference image is taken to be noise free (i.e. $\mathbf{dS}_{\mathbf{ref}} = 0$), the LSNR reconstruction may be seen to entail a simple substitution of an ideally modest artifact term for the leading noise term. By comparison, because of its global nature, the JE search of Larkman *et al*. effects a more complex transformation than the difference $\mathbf{s}'_{\text{ref}} - \mathbf{s}'$ in order to align the information content of the reference and reconstructed images. It should be noted that the use of a larger set of singular values/vectors for noise reduction in either the LSNR or JE technique will allow additional components of the reference image to enter into the reconstructed image, and will necessarily reduce the protection against replication of prior information.

Relation to Tikhonov regularization

Given the balance just described between noise reduction and replication of prior information, the LSNR technique may be classed as a regularization technique. Here, we identify the precise relationship between LSNR and the more familiar Tikhonov regularization strategy for the linear inverse problem of parallel image reconstruction.

A Tikhonov-regularized parallel image reconstruction takes the following form:

$$x = \min_x \left\{\| C (x - s) \|^2 + \lambda^2 \| x - x_{\text{ref}} \|^2\right\} \quad [6]$$

where λ is the regularization parameter.

Now assume that there is a λ such that $\lambda^2 \ll s_k$, $k \neq 1$ and $\lambda^2 \gg s_1$, and the reference image is noise free. Under these assumptions, it can be shown that the Tikhonov regularization result is:

$$x'_{\text{Tik}} = \Sigma_{k\neq 1}\,(v_k \otimes (u_k \cdot s)) + s_1^{-1}\,(v_k \otimes (u_1 \cdot s_{\text{ref}})) + s_1\lambda^{-2}\,(v_1 \otimes (u_1 \cdot (s' - s_{\text{ref}}))) + s_1\lambda^{-2}\,(v_1 \otimes (u_1 \cdot ds)) \quad [7]$$

whereas LSNR yields a result of:

$$x'_{\text{LSNR}} = \Sigma_{k\neq 1}\, s_k^{-1}\,(v_k \otimes (u_k \cdot s)) + s_1^{-1}\,((v_1 \otimes (u_1 \cdot s_{\text{ref}}))) \quad [8]$$

It is clear that Tikhonov regularization has an additional term $s_1\lambda^{-2}(\mathbf{v_1}\otimes(\mathbf{u_1}\cdot(s'-s_{\text{ref}})))$ containing the difference between the original image and the reference image, as well as an additional noise term $s_1\lambda^{-2}(v_1\otimes(\mathbf{u}_1\cdot\mathbf{ds}))$.

The first term can be further combined with the projected reference contribution term $s_1^{-1}\,(v_1 \otimes (u_1 \cdot s_{\text{ref}}))$ to have a signal component in the first principal component of $s_1\lambda^{-2}\,(v_1 \otimes (u_1 \cdot s')) + \left(s_1^{-1} - s_1\lambda^{-2}\right)(v_1 \otimes (u_1 \cdot s_{\text{ref}}))$. In other words, unlike LSNR, which purely uses the projected signal component from the reference image, Tikhonov regularization balances noise reduction and artifact generation by retaining a portion (multiplied by $s_1\lambda^{-2}$) of the original signal and noise, and reducing by a similar amount the presence of the corrupting signal from the reference. The additional noise contribution is a byproduct of seeking a balance in the signal component between the original image and the reference image.

It should be noted that, under the assumption $\lambda^2 \ll s_k$, $k \neq 1$ and $\lambda^2 \gg s_1$, the information associated with the first principal component $s_1^{-1}\,(v_k \otimes (u_1 \cdot s_{\text{ref}})) + s_1\lambda^{-2}\,(v_1 \otimes (u_1 \cdot (s' - s_{\text{ref}}))) + s_1\lambda^{-2}\,(v_1 \otimes (u_1 \cdot ds))$ will still be dominated by $s_1^{-1}\,(v_k \otimes (u_1 \cdot s_{\text{ref}}))$. In other words, LSNR may also be understood as a rapid and automatic method for the selection of the optimal Tikhonov regularization parameter λ in the case of high accelerations, for which the control of noise is generally most critical.

METHODS

Effective noise reduction in accelerated images using our proposed LSNR approach was demonstrated for both phantom and *in vivo* image data (7). LSNR was demonstrated *in vivo* utilizing low-resolution reference images. Various acceleration schemes were explored and the performance of the proposed method was investigated for large numbers of coil elements. These studies were used to verify that the LSNR method does not replicate the reference image, and that small lesions which are conspicuous in a high-resolution image, but not discernible in a lower resolution reference image, were preserved after the application of the LSNR algorithm.

In vivo images

In vivo images were acquired in volunteers after obtaining written informed consent with the approval of our institutional review board. All images were acquired on a 1.5-TGE Excite HD-x scanner (GE Healthcare, Waukesha, WI, USA). Two-dimensional axial images of the brain were acquired using a head coil array with eight elements circumferentially

distributed. Brain images were acquired with T_1-weighted contrast by a spin-echo sequence with a single signal average and with T_2-weighted contrast by a fast spin-echo sequence with an echo train length of eight and with two signal averages. Acquisition parameters included: field of view, 22 cm; slice thickness, 5 mm; image matrix, 256 × 256; acquisition bandwidth, ±15.63 kHz; TR/TE = 500/20 ms for T_1 weighting; TR/TE = 2500/85 ms for T_2 weighting. Coil sensitivity maps for parallel imaging were obtained from the data in an autocalibrating manner (8,9). Low-resolution sensitivity estimates were obtained by Fourier transformation of the *k*-space center after filtering with a Kaiser-Bessel window ($\beta = 2$), before normalization by the square root of the sum of squares combination of the separate coil images. Low-resolution reference images were obtained in a similar fashion from a second equivalent acquisition, which therefore has independent noise content. In order to simulate accelerated acquisitions whilst still providing exact unaliased references for comparison, images were acquired fully sampled and later decimated with various acceleration factors. Undersampling in one direction and in two dimensions was investigated. To simulate two-dimensional acceleration, the frequency-encoded direction was undersampled after acquisition, mimicking the case of a section from a volumetric image acquisition. Maximal undersampling with acceleration factor R equal to the number of coils was investigated, using $R = R_{\text{phase}} \times R_{\text{freq}}$ equal to 4 × 2 and 2 × 4. In addition, the performance of the LSNR approach with submaximal acceleration was explored with various acceleration factors. Discrete lesions were simulated by setting the pixel intensities of four small regions to unity in a single two-dimensional axial SENSE-reconstructed image. These lesions were chosen in order to maximize their distribution throughout the parenchyma to fully explore whether the LSNR method leads to the disappearance or creation of new lesions as a result of aliasing and artifact creation.

Image reconstruction

Images were reconstructed using the Cartesian SENSE approach as described by Pruessmann *et al*. (1). Regularly undersampled data were reconstructed into aliased images by fast Fourier transformation. Unfolding was then achieved using the inverse of the sensitivity matrix found by singular value decomposition (SVD) for groups of aliased pixels (Equation [15]). SENSE image reconstruction was implemented with a coil sensitivity image mask, which was fully automatically constructed by Otsu's method (10), which chooses the threshold to minimize the intraclass variance of the black and white pixels, followed by morphological filling and dilation. Such a mask identifies the dark space or null content of the coil sensitivity image and allows for the pixels in this region to be set to zero value. The *g*-factor noise amplification is thereby reduced by eliminating aliased pixel positions from the reconstruction which are known to contribute no signal intensity from the object.

The LSNR algorithm was implemented on a pixel-by-pixel basis. The sensitivity matrix was formed from the known coil sensitivities and decomposed via SVD. The principal singular value and vector were then used to find δS_1 with the vector of unfolded image pixels and the corresponding vector of pixels in the reference image. Additional singular vectors could be used by finding noise reduction vectors for the singular vectors corresponding to the scaling parameters δS_k (Equation [15]) with $k > 1$.

Tikhonov regularization was also implemented in a similar manner to the LSNR algorithm, except that the regularization parameter λ was chosen *ad hoc* to be optimized at 0.01 after searching for a parameter ranging from 1 to 1×10^{-4} and examining *g*-factor data, difference images and visual quality.

Image evaluation

For the original SENSE images, the *g*-factor was calculated according to the analytical formula provided by Pruessmann *et al*. (1). For the LSNR method, noise reduction was calculated in a similar fashion, with reconstruction matrix elements modified as described in the Theory section above. In general, the *g*-factor for SENSE can be computed as:

$$g = \sqrt{\left[\left(C^{H}\Psi^{-1}C\right)^{-1}\right]_{\rho,\rho}\left(C^{H}\Psi^{-1}C\right)_{\rho,\rho}}, \quad [9]$$

with ρ denoting the index of the voxel under consideration within the set of voxels to be separated, and ψ denoting the sample noise matrix.

For the LSNR method, Equation [9] basically takes the same form, except that the encoding matrix C is replaced by the new matrix, assuming a noise-free reference image:

$$C_{\mathrm{LSNR}} = \Sigma_{k\neq 1} s_k^{-1} (\mathrm{v_k} \otimes \mathrm{u_k}) \quad [10]$$

Joint entropy

Comparison was performed between the LSNR approach and the JE search approach for identical datasets. All JE reconstructions were performed from coil sensitivity-masked SENSE-reconstructed images, with the same low-resolution reference image used in LSNR reconstructions. It should be noted that the JE method only converges to meaningful minima if the input SENSE and reference images are masked. The implementation of the JE search followed the general method described by Larkman *et al*. with some minor modifications. Specifically, for each set of aliased voxels *x*, δS_{Ref} was first calculated as described above. δS_{Ref} was then set as the center of a complex space whose real axis was bound from $-2\mathrm{Re}\{\delta S_{\mathrm{Ref}}\}$ to $+2\mathrm{Re}\{\delta S_{\mathrm{Ref}}\}$, and whose imaginary axis was bound in a similar manner from $-2\mathrm{Im}\{\delta S_{\mathrm{Ref}}\}$ to $+2\mathrm{Im}\{\delta S_{\mathrm{Ref}}\}$, defined by upper and lower bounds that were equal to the real and imaginary parts of δS_{Ref}, respectively. The space was distributed into a 22 × 22 grid of discrete coordinates. Each combination of real and imaginary values in this complex plane was then chosen as the δS_1 value, and the set of aliased voxels was noise reduced according to Equation [1]. The SENSE image was then updated with these new noise-reduced voxels, and a joint histogram, with a bin size of 40, of this updated SENSE image and the low-resolution reference image was then constructed using the `hist3' function in the Matlab Statistics Toolbox. JE was then calculated in the usual manner (4). The real and imaginary coordinate leading to the minimum JE was then chosen as the δS_1 value used in Equation [1] for the final JE noise-reduced image. This iterative process was continued for each *x* vector. It should be noted that certain parameters, such as the number of coordinates in the complex search space and joint histogram bin size, were determined in an *ad hoc* manner in an attempt to minimize algorithm runtime, as even small increments in these parameters would lead to significantly larger runtimes.

All image reconstruction and processing were performed on a standard PC laptop computer with a 1.7-GHz processor and 2 GB RAM using the Matlab programming environment (The Math-works, Natick, MA, USA).

RESULTS

In all noise reduction experiments, the LSNR algorithm required roughly 30 s to produce the noise-reduced image, approximately four orders of magnitude less time than the 95 h required for JE minimization.

Figure 1 shows T_1-weighted *In vivo* brain images which were acquired with an eight-element head array and reconstructed at various acceleration rates from 1 × 1 to 4 × 2 with reference images reconstructed with 96 *k*-space lines without further image-based artifact reduction. Significant noise reduction was achieved by the LSNR method without apparent direct replication of the reference image at a maximal acceleration rate of 4 × 2, as well as at submaximal acceleration rates, e.g. 3 × 2 and 4 × 1. By contrast, the original SENSE reconstruction was significantly degraded by noise amplification. At lower acceleration rates, noticeable artifacts caused by the difference of the original image and the low-resolution reference appeared, although, in these cases, the original SENSE reconstruction had a high signal-to-noise ratio as a result of data redundancy. These findings were confirmed by the *g*-factor maps, as shown in Fig. 2. The *g*-factors for LSNR reconstruction were much lower than for SENSE reconstruction alone, especially at high acceleration rates. It should be noted that LSNR yielded an average *g*-factor of 0.71 in the 3 × 1 case, demonstrating the noise suppression ability of the method. In Fig. 3, the error maps for the images in Fig. 1 are shown. The error maps were calculated by taking the absolute difference of the noise-free image and either the SENSE or LSNR image. It is noted that, for accelerations of 3 × 2 and 4 × 2, the average difference was less for the LSNR image compared with the SENSE image. For the 3 × 1 and 4 × 1 cases, the average difference was either increased or similar to the SENSE image. For Fig. 4, the studies were repeated in T_2-weighted brain images with 2 × 4 acceleration, yielding similar results. In order to examine how dominant the inverse encoding matrix was at different accelerations, in Fig. 5, the condition number, which is the ratio of the largest to smallest singular value, of the inverse encoding matrix (see Appendix A, Equation [11]) for the SENSE images in Fig. 1 was plotted against the acceleration factor. The condition number is a well-known metric of matrix stability, particularly during inversion. Next, four discrete simulated lesions were added to the SENSE-reconstructed image from Fig. 4, without adding lesions to the reference image, in order to further test the versatility of the LSNR method using a reference image of different features. A corresponding LSNR reconstruction was performed, and is shown in Fig. 6. The resulting LSNR image preserves the lesions without creating any visually appreciable artifacts. It should be noted that LSNR was also successful when using a reference image slightly displaced from the image slice, an observation that may have practical importance for situations in which sensitivity calibration scans are not perfectly aligned with accelerated scans.

A JE reconstruction, in Fig. 7, resulted in improved noise reduction, but increased aliasing artifacts, when compared with the LSNR image in the center of the figure. JE between the reference image and the noise-reduced image was reduced by 41% when compared with JE between the reference image and the input SENSE-reconstructed image; 20% of all JE searches during the reconstruction converged to a minimum δS value that was equal to δS_{Ref} calculated by the LSNR method. Moreover, in Fig. 7, a Tikhonov regularization was performed which did not yield significant noise reduction compared with either LSNR or JE methods.

In Fig. 8, the effect of reference image resolution on LSNR image quality is illustrated. The use of the LSNR method with a reference image with 32 phase-encoded lines resulted in noise reduction, but at the cost of introducing a noticeable edge aliasing artifact compared with a reference image of 96 phase-encoded lines. This artifact was derived chiefly from

high-intensity edge regions of the SENSE image, such as the pericalvarial tissues (PCTs); these are defined as the tissues surrounding the skull, which consist of the scalp and its five layers, and the bony cranium. In general, by lowering the resolution of the reference image, edges are blurred as high-frequency data are decimated, leading to the broadening of high-intensity areas, such as the PCTs. This can be conceptualized by considering that, if the reference and target images were superimposed, there would be overlap of the blurred edges of the reference image, such as the high-intensity regions of the skull, on nonedge, lower intensity areas of the target image, leading to an increase in the value of the difference between the reference and the true aliased signals, as shown in Equation [5], thereby causing an aliasing artifact when the target image is unfolded. As shown in Fig. 8, removal of these high-intensity regions from the LSNR process resulted in the elimination of most of the residual artifacts. PCT removal was performed by an automated segmentation method in which: (i) masked SENSE images were used to identify the brain parenchyma without PCTs; (ii) our LSNR technique was performed on the remaining image without PCTs; and (iii) PCTs from the original masked SENSE images were added back to the LSNR-reconstructed image. Specifically, following the masked SENSE reconstruction as described above, an extended minima transform was performed on each masked SENSE image using a connectivity of eight points to create a binary image differentiating the total image (PCT and brain parenchyma) from nontissue (image nullspace). The brain parenchyma was isolated from the masked SENSE reconstruction by exploiting the fact that the PCT in the image is surrounded at its exterior and interior by an area of low intensity that has greater than four-point connectivity. By excluding the image nullspace and the PCT, the LSNR technique was performed on only the brain parenchyma from the masked SENSE image. Finally, using simple image addition, the PCT from the masked SENSE image was reintroduced to this brain tissue LSNR image, resulting in an LSNR hybrid image. LSNR images showed a marked reduction in edge artifact after removal of PCT (middle right in Fig. 8) or increasing the reference image resolution (right image in Fig. 8).

DISCUSSION AND CONCLUSIONS

Using the LSNR method, we were able to reduce *g*-factor-related noise in highly accelerated scans when reference and target images were of similar contrast. Although the method relies on prior information in the form of a reference image, the algorithm remains substantially protected against simple replication of reference image content, as aliased sets of voxels may only be changed in fixed ratios as defined by the singular vectors v_k. This prevents unrestricted modification of any given pixel value to match prior information. Moreover, lesions added to the SENSE image, but not to the reference image, were preserved in LSNR reconstructions. Noise reduction using our least-squares approach was, on average, four orders of magnitude faster than the algorithmically challenging JE approach, but yielded similar results for a single δS_1 value. Like our LSNR implementation, our JE implementation used uncompiled Matlab code, and some significant reductions in reconstruction time are expected to be possible. However, JE reconstructions would still be expected to occupy hours rather than seconds. Moreover, the inefficiency of the JE method was further confirmed by the fact that 20% of all the JE search iterations converged on the same δS_1 value as the LSNR method, although this may be confounded by the fact that the iteration centered around δS_1.

Moreover, as shown in Fig. 7, the results obtained by implementing a Tikhonov regularization are slightly improved from the SENSE image, but are not as effective in noise reduction as either the LSNR or JE methods. It should also be noted that the regularization parameter λ, as a well-known issue, is not easy to determine for each simulation, depending on the image and acceleration factor. Given the choice of parameter and optimization difficulties, the Tikhonov method appears to be the lesser choice for noise reduction, as it is

not as simple as the LSNR method, nor is it as versatile as the JE method in its ability to use a reference image of different contrast. Further, the Tikhonov method importantly showed significantly less noise reduction when compared with both the LSNR and JE techniques. Based on the formulation of the Tikhonov regularization and its relationship to the LSNR technique as outlined in the Theory section, it would appear that the LSNR method is a rapid and automatic method for choice of the Tikhonov regularization parameter.

Despite the efficacy of the LSNR method for highly accelerated data where SENSE reconstruction is poorly conditioned, in better conditioned cases, the LSNR method using one singular value showed a less satisfactory performance (Figs 1 and 3). As expected from theory, in Fig. 5, as the acceleration factor increases, the condition number of the inverse encoding matrix (defined in Appendix A, Equation [11]) increases exponentially. This is confirmed empirically by our results, which show that, unless the inverse encoding matrix is poorly conditioned, such as the eight-fold acceleration case, there will not be a sufficiently dominant singular value, and thus, although the single-value LSNR method will still yield noise reduction, it will be at the expense of an increased artifact. At the same time, as the number of aliased voxels decreases, the protection against the replication of prior information is reduced, which also accounts for increased levels of artifact at lower acceleration factors. This is a clear limitation of the LSNR method.

The LSNR approach allows for the incorporation of multiple singular values/vectors for each set of aliased voxels, with the important caveat that, as more components are used, the result is less effectively protected against the replication of prior information from the reference image. If all components are used then, as shown in Equation [3], the terms cancel and $x'_{LSNR} = x_{ref}$. Also of note, due to the dramatically increased computational burden for a multidimensional search, the JE method is currently practical only for the determination of a single δS_1.

It should be stated that the LSNR method works best when target and reference images are of the same contrast, which is intuitive based on theory, as the method involves a subtraction between the reference image and the SENSE image. Thus, it is conceivable that a reference image of different contrast would skew the LSNR calculation. This stipulation is in distinction from the JE method, which is more global, in that it can technically operate with a reference image of any contrast, as the algorithm is based on image structures rather than image intensity.

A major source of residual artifact in the brain images when using a low-resolution reference image is the PCT, which produces characteristic edge artifacts across the image. These edge artifacts are mainly a result of omitted high-frequency data, especially for bright edges, in the undersampled low-resolution reference images used by LSNR. These artifacts are introduced by the LSNR method from the reference image based on aliasing patterns of a given acceleration. This is a limitation of the method, which can be solved by two approaches.

The first and most straightforward method is to increase the resolution of the reference images. This approach can be easily adopted in applications in which a series of images are acquired to study the dynamics of the subject, such as functional MRI.

The second approach is to utilize image analysis techniques to segment and remove the regions with sharp bright edges, such as PCT, and then apply the LSNR technique on the image without PCT. It should be noted that this generally does not lead to a severe compromise in noise reduction for the areas of the image with sharp bright edges, such as PCT, given that the signal intensity in these regions is higher than in the rest of the image. Figure 8 illustrates these two approaches on a 3 × 2 accelerated T_1-weighted image. Clearly,

without the segmentation method, the artifacts in the LSNR image using a 32-line reference image are severe. However, both the image with brain parenchyma masking using a 32-line reference, and the image without brain parenchyma masking using a 96-line reference image exhibit effective noise removal without the introduction of significant edge artifacts in the reconstructed images.

At present, the LSNR method has only been applied for regular Cartesian undersampling, although the algorithm is sufficiently efficient that other sampling trajectories might also be considered. As the LSNR approach is highly effective at reducing noise for any image that is poorly conditioned, the method could provide a means for automatic noise reduction when applied to a maximally accelerated SENSE reconstruction. Moreover, the approach could also be applied selectively to areas of an image (i.e. to subsets of aliased voxels) for which the condition number of the reconstruction matrix rises above a defined threshold.

In conclusion, the principal component LSNR approach proposed here is a promising candidate for rapid noise reduction in highly accelerated images or dynamic imaging, and a rapid alternative method to the JE approach with slightly increased constraints on the reference images.

Supplementary Material

Refer to Web version on PubMed Central for supplementary material.

Acknowledgments

This work was supported by National Institutes of Health (NIH) Grant R01-EB002568 (high-performance high-field parallel MRI).

APPENDIX A

Cartesian sensitivity encoding (SENSE) image reconstruction with regular undersampling involves the inversion of an encoding matrix C composed of complex coil sensitivities at each set of aliased positions in the target image. C can be factorized using a singular value decomposition (SVD) as $C = USV^{+}$, with U and V as unitary matrices and S as a diagonal matrix. The superscript `+' indicates Hermitian conjugation. By generalizing the notation of Larkman *et al*., the inverse matrix, or reconstruction matrix, can be written as:

$$C_{inv} = VS^{-1}U^{+} = \Sigma_k s_k^{-1} (v_k \otimes u_k) \quad [11]$$

where v_k and u_k are columns and rows of the *V* and U^{+} matrices, respectively, s_k is the kth diagonal element of the diagonal *S* matrix and the sum over *k* runs from unity to the acceleration factor. If the unfolded pixels are represented in a complex vector:

$$x = x' + dx \quad [12]$$

with true pixel intensity x and noise contribution *dx*, and the folded pixels are represented in a complex vector:

$$s = s' + dS \quad [13]$$

once again separating the true pixel intensity s′ from the noise contribution ds, the SENSE-reconstructed image (i.e. the complete image with amplified noise) is:

$$x = C_{inv} s \quad [14]$$

and the true noise-free image intensity is:

$$\begin{aligned} x' &= x - dx = x - C_{inv} ds \\ &= x - \Sigma_k s_k^{-1} (v_k \otimes (u_k \cdot ds)) \equiv x - \Sigma_k \left(s_k^{-1} \delta S_k \right) v_k \end{aligned} \quad [15]$$

Here, δS_k is an unknown scalar value defined by the inner product of the kth vector u_k with the unknown noise vector ds. It should be noted that, when all singular values are equal, slight perturbations in the measured data do not impact significantly on the reconstructed image. In this case, C is well conditioned, with a condition number (defined as the ratio between the largest and smallest singular values) equal to the ideal value of unity. However, if one of the singular values of C is much smaller than the others, the corresponding singular value of C_{inv} will be very large. In this case, C_{inv} is considered to be ill-conditioned and will have a condition number much greater than unity. Thus, even a small perturbation in the data, in the form of noise, will result in a large difference in the reconstructed image, provided that the perturbation has some component along the direction of the singular vector associated with this large singular value (5). It is known that, at high accelerations, the encoding matrix C becomes ill-conditioned. As a result, C_{inv} is dominated by the first few singular values and singular vectors. Thus, only one or a small number of complex quantities δS_k need to be found to estimate the noise-free image intensities.

Abbreviations used

JE	joint entropy
LSNR	least-squares noise-reduced
PCT	pericalvarial tissue
SENSE	sensitivity encoding
SVD	singular value decomposition

REFERENCES

1. Pruessmann KP, Weiger M, Scheidegger MB, Boesiger P. SENSE: sensitivity encoding for fast MRI. Magn. Reson. Med. 1999; 42(5):952–962. [PubMed: 10542355]
2. Tsao, J.; Boesiger, P.; Pruessmann, KP. Noise normalization by variable filtering in parallel imaging and conventional imaging with inhomogenous coils. 11th Annual Meeting ISMRM; Toronto, ON, Canada. 2003. p. 780
3. Lin FH, Kwong KK, Belliveau JW, Wald LL. Parallel imaging reconstruction using automatic regularization. Magn. Reson. Med. 2004; 51(3):559–567. [PubMed: 15004798]
4. Larkman DJ, Batchelor PG, Atkinson D, Rueckert D, Hajnal JV. Beyond the g-factor limit in sensitivity encoding using joint histogram entropy. Magn. Reson. Med. 2006; 55(1):153–160. [PubMed: 16342149]
5. Larkman DJ, Nunes RG. Parallel magnetic resonance imaging. Phys. Med. Biol. 2007; 52(7):R15–R55. [PubMed: 17374908]
6. Patel AS, Duan Q, Robson PM, McKenzie CM, Sodickson DK. A simple noniterative principal component technique for rapid noise reduction in parallel MR images. United States Patent Application No. 12/152,940. May 19.2008

7. Patel, AS.; Duan, Q.; Robson, PM.; McKenzie, CM.; Sodickson, DK. A simple noniterative principal component technique for rapid noise reduction in parallel MR images. 15th Annual Meeting ISMRM; Berlin, Germany. 2007. p. 980

8. McKenzie CA, Yeh EN, Ohliger MA, Price MD, Sodickson DK. Self-calibrating parallel imaging with automatic coil sensitivity extraction. Magn. Reson. Med. 2002; 47(3):529–538. [PubMed: 11870840]

9. Sodickson DK, McKenzie CA. A generalized approach to parallel magnetic resonance imaging. Med. Phys. 2001; 28(8):1629–1643. [PubMed: 11548932]

10. Otsu N. A threshold selection method from gray-level histograms. IEEE Trans. Syst. Man Cybernet. 1979; 9(1):62–66.

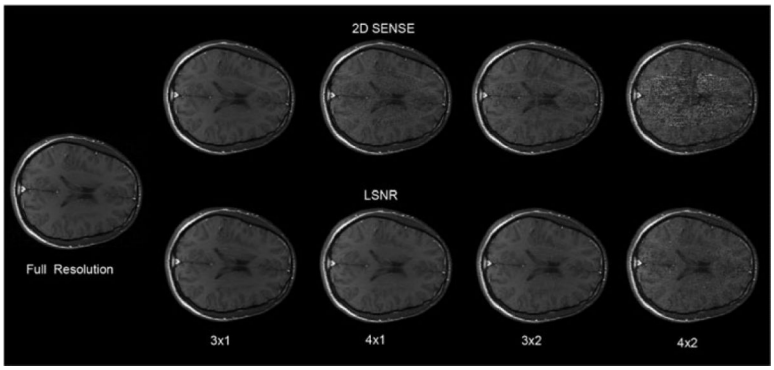

Figure 1.

In vivo T_1-weighted brain images (matrix size, 256 × 256) obtained with an eight-element head array. Top row: standard sensitivity encoding (SENSE) reconstruction. Bottom row: least-squares noise-reduced (LSNR) reconstruction. From left to right: various acceleration rates from 1 × 1 (i.e. unaccelerated gold standard) to 4 × 2. A reference image of matrix size 96 × 96 was used for LSNR reconstruction.

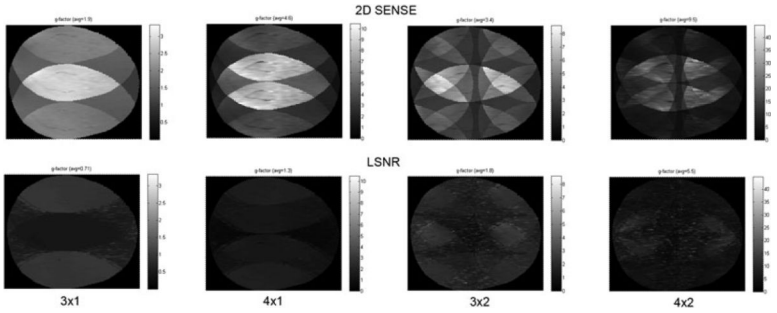

Figure 2.

In vivo-factor maps corresponding to the accelerated images of Fig. 1. Top row: standard sensitivity encoding (SENSE) reconstruction. Bottom row: least-squares noise-reduced (LSNR) reconstruction. From left to right: various acceleration rates from 3 × 1 to 4 × 2.

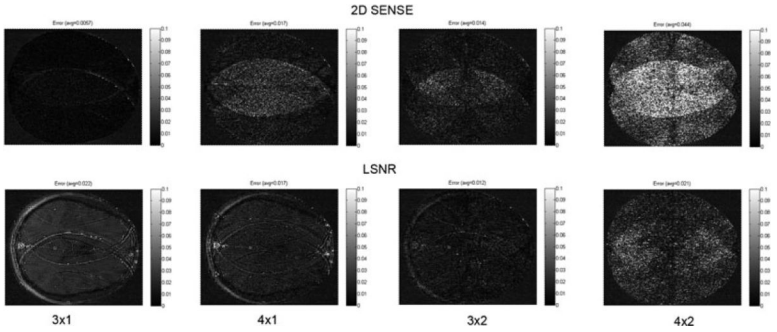

Figure 3.
In vivo difference images corresponding to the accelerated images of Fig. 1. Top row: standard sensitivity encoding (SENSE) reconstruction. Bottom row: least-squares noise-reduced (LSNR) reconstruction. From left to right: various acceleration rates from 3 × 1 to 4 × 2.

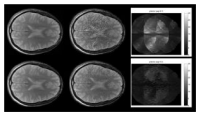

Figure 4.
In vivo T_2-weighted brain images obtained with the eight-element head array. Top left: unaccelerated gold standard (matrix size, 256 × 256). Top middle: 2 × 4 sensitivity encoding (SENSE) reconstruction (matrix size, 256 × 256). Top right: SENSE *g*-factor map. Bottom left: low-resolution reference image (matrix size, 96 × 96). Bottom middle: least-squares noise-reduced (LSNR) reconstruction (matrix size, 256 × 256). Bottom right: LSNR *g*-factor map.

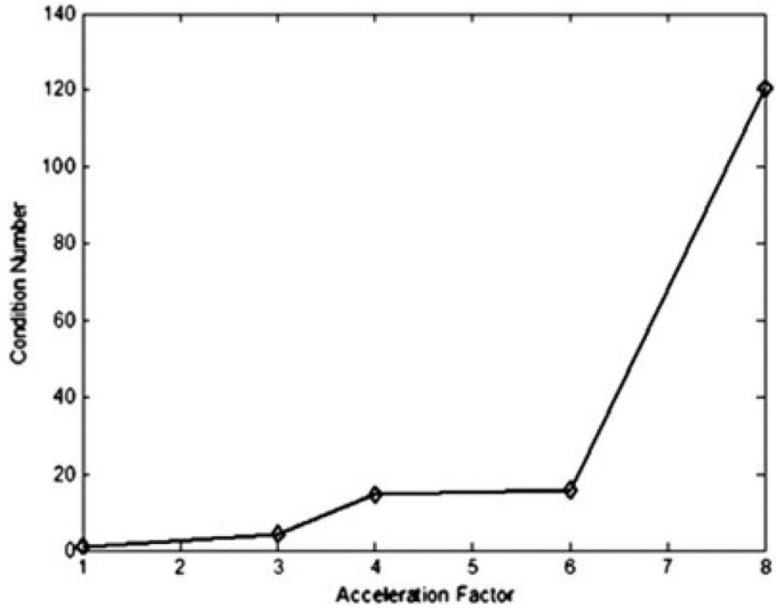

Figure 5.
Condition number of the inverse encoding matrix for the sensitivity encoding (SENSE) images in Fig. 1 plotted against the acceleration factor.

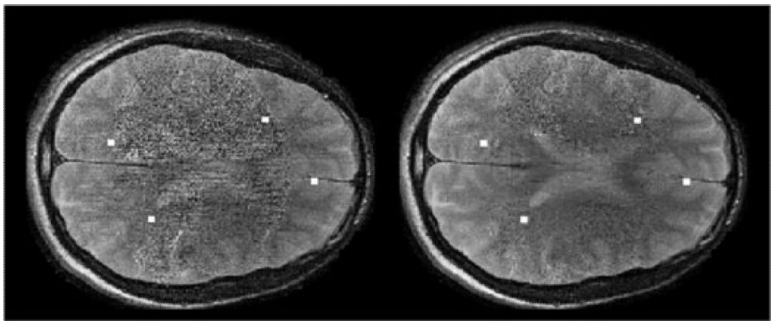

Figure 6.
In vivo T_2-weighted brain images (matrix size, 256 × 256) with artificially added `lesions'. Left: 2 × 4 sensitivity encoding (SENSE) reconstruction with four lesions added. Right: least-squares noise-reduced (LSNR) reconstruction, preserving lesions not present in the 96 × 96 reference image.

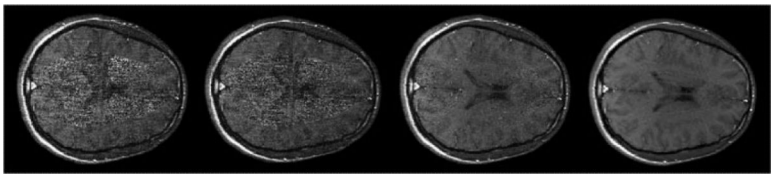

Figure 7.
Comparison of reconstruction strategies for *in vivo* T_1-weighted brain images (matrix size, 256 × 256): Left: 4 × 2-accelerated masked sensitivity encoding (SENSE) reconstruction. Middle left: Tikhonov reconstruction. Middle right: least-squares noise-reduced (LSNR) reconstruction. Right: joint entropy (JE) reconstruction using the same 64 × 64 reference image.

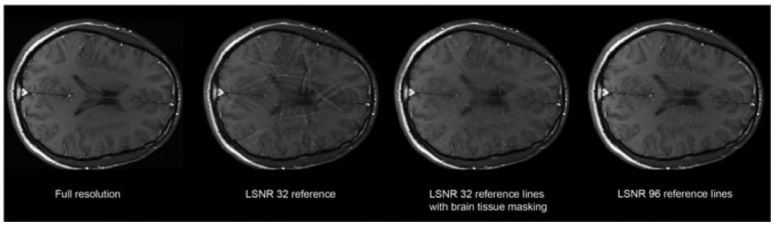

Figure 8.
In vivo T_1-weighted brain images obtained with an eight-element head array at 3 × 2 acceleration. Left: full-resolution source image. Center left: least-squares noise-reduced (LSNR) reconstruction using a 32 × 32 reference image. Center right: LSNR reconstruction using a 32 × 32 reference image combined with pericalvarial tissue masking. Right: LSNR reconstruction using a 96 × 96 reference image.